

Josephson dynamics of bicrystal d -wave $\text{YBa}_2\text{Cu}_3\text{O}_{7-\delta}$ dc-SQUIDS

T. Lindström,* J. Johansson, T. Bauch, E. Stepantsov, and F. Lombardi

Quantum Device Physics Laboratory, Department of Microtechnology and Nanoscience, Chalmers University of Technology, SE-412 96 Göteborg, Sweden

S. A. Charlebois

Département de Génie Électrique et de Génie Informatique, Université de Sherbrooke, Sherbrooke, Canada

(Received 3 February 2006; published 6 July 2006)

The properties of $\text{YBa}_2\text{Cu}_3\text{O}_{7-\delta}$ dc-SQUIDS (superconducting quantum interference devices) with 0° – 45° grain boundary junctions have been studied. Structures fabricated on two types of bicrystals have been investigated: The conventional [001]-tilt type and a novel configuration with both [001] and [100] tilt. Measurements have been performed in the temperature range 50 mK–30 K. We find that the complicated dynamics of these SQUIDS can be understood if the effects of the predominant d -wave symmetry on the current transport is taken into account. In particular the presence of a second-harmonic current component in the current phase relation and the inclusion of π -facets in the grain boundary are shown to be important effects. We also find that by increasing the [100] tilt of the grain boundary it is possible to increase the quality factor of the SQUIDS without reducing the magnitude of the second-harmonic current component. A simple model, which includes the effects of faceting of the grain boundary and the presence of a second-harmonic current component, is shown to be in qualitative agreement with our results.

DOI: 10.1103/PhysRevB.74.014503

PACS number(s): 85.25.Cp

I. INTRODUCTION

By now it is well established that the predominant d -wave symmetry of the pairing wave function in high- T_c superconductors can influence the current-phase relation (CPR) of Josephson junctions.¹ The four lobes of the pairing wave function in a pure d -wave superconductor have alternating signs and are separated by nodes where the superconducting gap vanishes. Furthermore, the symmetry follows that of the a and b axes of the crystal lattice which makes it possible to design interfaces where the tunneling occurs from a node to a lobe (Fig. 1). In this configuration, the ordinary Josephson current will be suppressed and ideally zero in a junction with a perfect interface. In these so-called 0° – 45° junctions there is however another transport channel for the supercurrent, namely transport mediated by zero-energy Andreev bound states at the junction interface.² Quasiparticles can be reflected from a positive to a negative lobe leading to the net transfer of a Cooper pair. The resulting Josephson current has twice the periodicity in phase compared to that of a conventional junction $I(\phi) = I^{\text{II}} \sin 2\phi$.^{3,4}

Grain boundary (GB) junctions⁵ have been successfully used to study these effects⁶ and have largely confirmed theoretical predictions. However, due to imperfections in the interface there are effectively many parallel transport channels and the exact shape of the CPR in each channel will depend on local properties such as transparency and the shape of the tunneling cone. Furthermore, if the local misorientation angle deviates more than a few degrees from 0° to 45° the symmetry argument outlined above is not valid; some conduction channels will carry conventional Josephson current without a π -periodic component. Hence, the effective CPR for the whole junction has the form

$$I = I^{\text{I}} \sin \phi - I^{\text{II}} \sin 2\phi = I^{\text{I}}(\sin \phi - \alpha \sin 2\phi), \quad (1)$$

where $\alpha = I^{\text{II}}/I^{\text{I}}$. The negative sign of the second harmonic is a direct consequence of the symmetry in 0° – 45° junctions.

Other orientations of the electrodes may give a positive second harmonic.⁷ Moreover, in principle there are also higher order terms ($\sin 3\phi, \sin 4\phi, \dots$) but the relative magnitude of those will always be very small in real GB junctions which justifies retaining only the first two terms.

It should be noted that higher harmonics contribute to the CPR also in conventional junctions.⁸ The contribution is, however, extremely small unless the transparency is close to 1. The mechanism is also completely different from that in 0° to 45° high- T_c junctions where we can have $I^{\text{II}} > I^{\text{I}}$, which is not possible in a conventional junction.

Recently an alternative explanation for the appearance of a strong second-harmonic current component in 0° – 45° YBCO junctions was proposed.⁹ However, the form of Eq. (1), and therefore the theory outlined in this work, is independent of the details of the microscopic theory.

In order to detect the presence of higher harmonics in the CPR a phase-sensitive measurement technique is usually employed.⁶ By carefully studying their dynamics it is possible to directly see the effect even in single junctions,¹⁰ but direct measurements on phase sensitive devices give more direct information. We have previously shown¹¹ that a strong

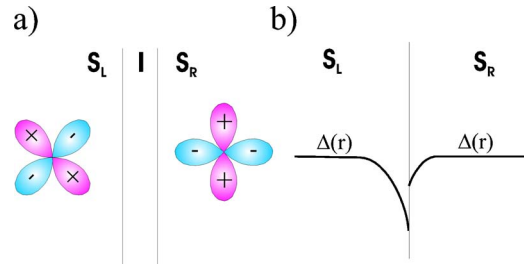


FIG. 1. (Color online) The shape of the pairing wave function (a) and the magnitude of the gap (b) in a specular two-dimensional 0° – 45° high- T_c junction.

second harmonic in the CPR affects the dynamics of ordinary dc-SQUIDs (superconducting quantum interference devices). Similar results have later been presented by Schneider *et al.*¹² Gardiner *et al.* have presented data obtained from measurements on rf-SQUIDs.¹³

The main reason for the interest in 0° – 45° dc-SQUIDs is that it has been suggested that they may potentially be used as “silent” qubits¹⁴ since the ground state energy is double degenerate at zero field. Realization of this HTS qubit requires junctions with a high quality factor and an unconventional CPR with a well pronounced second-harmonic component (note, however, that the effects of a second-harmonic current component can be clearly visible in the SQUID dynamics even for values of α that do not lead to the formation of a double well¹⁵). Recent theoretical work^{16,17} has also shown that “intrinsic” *d*-wave effects such as quasiparticle dissipation via zero-energy states are likely to be much less detrimental than has been previously feared. The demonstration of macroscopic quantum tunneling¹⁰ and resonant activation¹⁸ in 0° – 45° biexptial junctions has shown that it is indeed possible to use these junctions in the quantum regime.

In this paper we present results that address three topics relevant for the understanding of 0° – 45° SQUIDs and the usability of such systems in the quantum limit.

(1) What determines the quality factor of a bicrystal Josephson junction? From studies of biepitaxial junctions¹⁹ it is known that a strong *c*-axis component in the tunneling often results in underdamped junctions which make them ideal for studies and applications in the quantum limit. Here we study in more detail the effect of the *c*-axis tunneling component on the quality factor of SQUIDs. Results obtained from devices fabricated on conventional [001]-tilt bicrystals are compared to those from SQUIDs fabricated on a novel type of bicrystal with *both* [001] and [100] tilt. Junctions with only [100] tilt have been studied previously^{20,21} and were shown to exhibit good properties.

(2) What is the temperature dependence of the second harmonic in the CPR? The onset temperature of the second-harmonic component in the CPR is predicted to depend on the barrier transparency of the Josephson junction or SQUID.¹ Here we study the effect of the second-harmonic component on the magnetic diffraction pattern of SQUIDs with various barrier transparencies at various temperatures.

(3) Is it possible to determine the second-harmonic components in the CPR of the two junctions in a SQUID from magnetic diffraction patterns? From the magnetic diffraction pattern of a SQUID it is not possible to determine a univocal set of second-harmonic components without using special phase retrieval algorithms but by measuring the critical currents of the two junctions of the SQUID independently we are able to unambiguously determine the second-harmonic components in a SQUID.

This paper is divided into five parts. In Sec. II we describe a general theory for the Josephson dynamics of 0° – 45° dc-SQUIDs. Section III describes the fabrication methods used. In Sec. IV we investigate how the properties of 0° – 45° junctions and SQUIDs change with increasing [100] tilt. Section V describes an experiment performed on a dc-SQUID with three electrodes where we show that junction parameters ex-

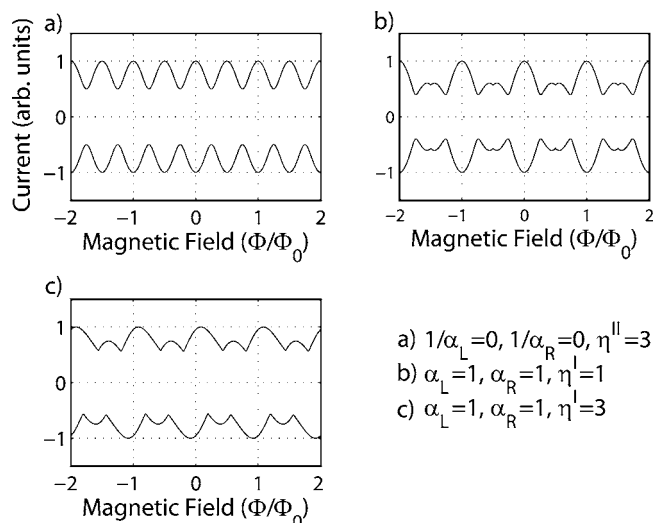


FIG. 2. Plots of I_c vs ϕ patterns that can result from the addition of a second harmonic to the CPR. The patterns have been normalized to have the same maximum I_c . We have used $\eta^I = I_R^I/I_L^I$, $\eta^{II} = I_R^{II}/I_L^{II}$, and $\alpha_{L,R} = I_{L,R}^{II}/I_{L,R}^I$.

tracted from the SQUID dynamics are consistent with measurements on the individual junctions. Finally, in Sec. VI experiments on the temperature dependence of the SQUID dynamics in the range 50 mK to 30 K are presented

II. THEORY

In this section we will outline a qualitative theory that captures the essential physics of the complex dynamics of high angle GB Josephson junctions and SQUIDs. The model is in agreement with measurements and incorporates the effects of faceting of the GB and a $\sin 2\phi$ current component in the CPR.

When two junctions with a CPR given by Eq. (1) are integrated in a loop, the resulting dc-SQUID has properties that differ significantly from what is found in conventional devices. Assuming the inductance of the SQUID loop can be neglected, the expression for the total current through the SQUID, $I_s(\phi, \phi_x)$, can be written

$$I_s(\phi, \phi_x) = I_L^I(\sin \phi - \alpha_L \sin(2\phi)) + I_R^I(\sin(\phi + \phi_x) - \alpha_R \sin 2(\phi + \phi_x)), \quad (2)$$

where the subscripts *L* and *R* denote the left and right arms of the SQUID, respectively, and ϕ_x is the phase difference between the junctions that is caused by the magnetic flux threading the SQUID loop. The critical current of the SQUID can then be calculated from Eq. (2) using

$$I_c(\phi_x) = \max_{-\pi < \phi < \pi} I_s(\phi, \phi_x). \quad (3)$$

These simple equations can give rise to a wide variety of I_c vs ϕ patterns, as shown in Fig. 2.

The most obvious effect of the $\sin 2\phi$ term is the appearance of π -periodic features in the patterns. However, unless the SQUID is asymmetric, the effects are quite subtle with

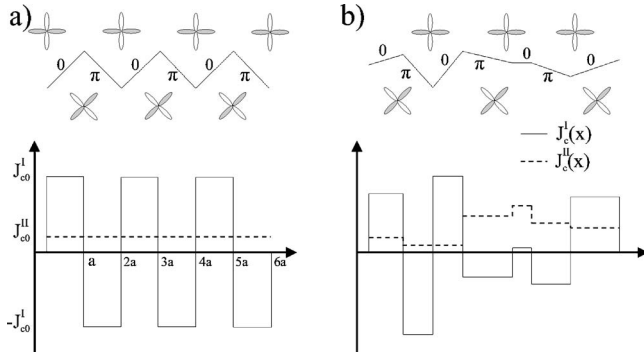


FIG. 3. Schematic representation of the grain boundary and its current distribution. (a) A so called zig-zag junction treated in example d . (b) A stochastic interface and the corresponding current distribution.

the exception for the periodicity which changes [Fig. 2(a)]. In the extreme case where there is no first harmonic in the CPR (corresponding to junctions with perfect interfaces) the SQUID modulation becomes purely π -periodic. Other combinations of parameters result in a reduced modulation depth and a maximum at nonzero field. The latter can, however, be difficult to distinguish from the effect of the inductance, L , of the SQUID-loop unless special precautions are taken to ensure that $LI_c/\Phi_0 \ll 1$. The effects are more evident if the SQUID is asymmetric, i.e., the left and right junctions have different values of I_c and/or α . Note that the maximum of the extra “hump” is not generally located at $\Phi_0/2$. Regardless of the parameters, the patterns are always point symmetric with respect to zero field.

We showed in a previous letter¹¹ that this simple theory can be used to explain the properties of 0° – 45° dc-SQUIDs as long as the field modulation of the junctions themselves can be neglected. If this is not the case, the situation becomes more complicated. Faceting of the GB plays an important role and happens at two length scales: Meandering creates facets that are typically 100–200 nm long and there is also microfaceting which is related to the lattice structure and has a typical length scale of 1–2 nm.²² Due to the d -wave symmetry the local properties of the GB depend strongly on the misorientation angle.²³

An important consequence of the meandering is the presence of so-called π -facets in the GB. Ideally, the 0° – 45° misorientation should result in a node-lobe arrangement of the order parameter in the electrodes (Fig. 1) but since the GB meanders, the exact arrangement varies. In some of these facets the arrangement will be, e.g., plus-plus and in some plus-minus. This means that the phase difference across the GB due to the d -wave symmetry will be shifted by π in some places resulting in a *negative* Josephson current density. Note that this does not necessarily imply a *circulating* current along the GB as long as the junction width d is much smaller than the Josephson penetration depth λ_J . This is of course a simplified picture but it captures the essential physics of the current transport in a d -wave GB junction. A more realistic model would also need to take into account, e.g., the shape of the tunneling cone and local variations of the interface properties.²⁴ But regardless of the details of the model, J_c

varies both in amplitude and sign as we move along the GB. This results in very complex dynamics.

To summarize, the meandering of the grain boundary results in a number of phenomena that need to be taken into account.

- Conventional Josephson currents, presumably due to tunneling via low-angle facets.
- Transport via bound Andreev states, resulting in a large second-harmonic component in the CPR.
- *Negative* currents due to the inclusion of π -facets in the grain boundary.

It is possible to extend the conventional model of Josephson junctions to include both the effects of faceting—including π -facets—and a second-harmonic component in the CPR. The meandering of the bicrystal is stochastic and, hence, it is difficult to directly extract detailed information about the GB from the properties of a real SQUID. Nevertheless, this simple model can be used to reach a qualitative understanding. A similar model has been presented by Kornev *et al.*²⁵ Multichannel models of GB have also been discussed by, e.g., Neils²⁶ and Lazarides,²⁷ but without taking into account the possibility of a second-harmonic in the CPR.

Following the usual method of deriving the equation that governs the behavior of a magnetically short junction in a perpendicular magnetic field B ²⁸ we introduce

$$\delta\phi = 2\pi \frac{2\lambda B}{\Phi_0} \delta z \rightarrow \phi(z) = 2\pi \frac{2\lambda B}{\Phi_0} z + \phi_0. \quad (4)$$

We also introduce $J_{k=L,R}^I(z)$, $J_{k=L,R}^{II}(z)$, the current densities for the first and second harmonics as we move along the GB in the left and right SQUID arm. The thickness w of the junction is assumed negligible compared to the London penetration depth λ . We can write the field dependent critical current of a dc-SQUID as

$$I_s(\phi_x) = \max_{-\pi < \phi_0 < \pi} \left\{ w \int_0^{d_L} J_L^I(z) \sin \phi(z) - J_L^{II}(z) \sin 2\phi(z) dz \right. \\ \left. + w \int_0^{d_R} J_R^I(z) \sin(\phi(z) + \phi_x) \right. \\ \left. - J_R^{II}(z) \sin 2(\phi(z) + \phi_x) dz \right\}, \quad (5)$$

where ϕ_x is the normalized external flux $2\pi BA/\Phi_0$, A being the area of the SQUID-loop and $d_{L,R}$ is the width of the left and right junction, respectively.

In SQUIDs with distributed junctions the resulting I_c vs ϕ pattern is a combination of the SQUID and junction response to the applied field. The simplest case in the absence of any interface inhomogeneities is when the SQUID response is modulated by the junction envelope but the general result is more complicated. Here we will give a few examples.

a. $J_{k=L,R}^I(z) = J_{c0}^I$, $J_{k=L,R}^{II}(z) = 0$. Equation (5) reduces to the familiar expression for the magnetic diffraction pattern of a conventional junction modulated by the SQUID response $2I_{c0} |\sin(\pi\Phi/\Phi_0)| / |\pi\Phi/\Phi_0| \cdot |\cos(\phi_x/2)|$.

b. $J_L^I(z) = J_{c0}^I$, $J_R^I(z) = -J_{c0}^I$, $J_{k=L,R}^{II}(z) = 0$. This is a model of

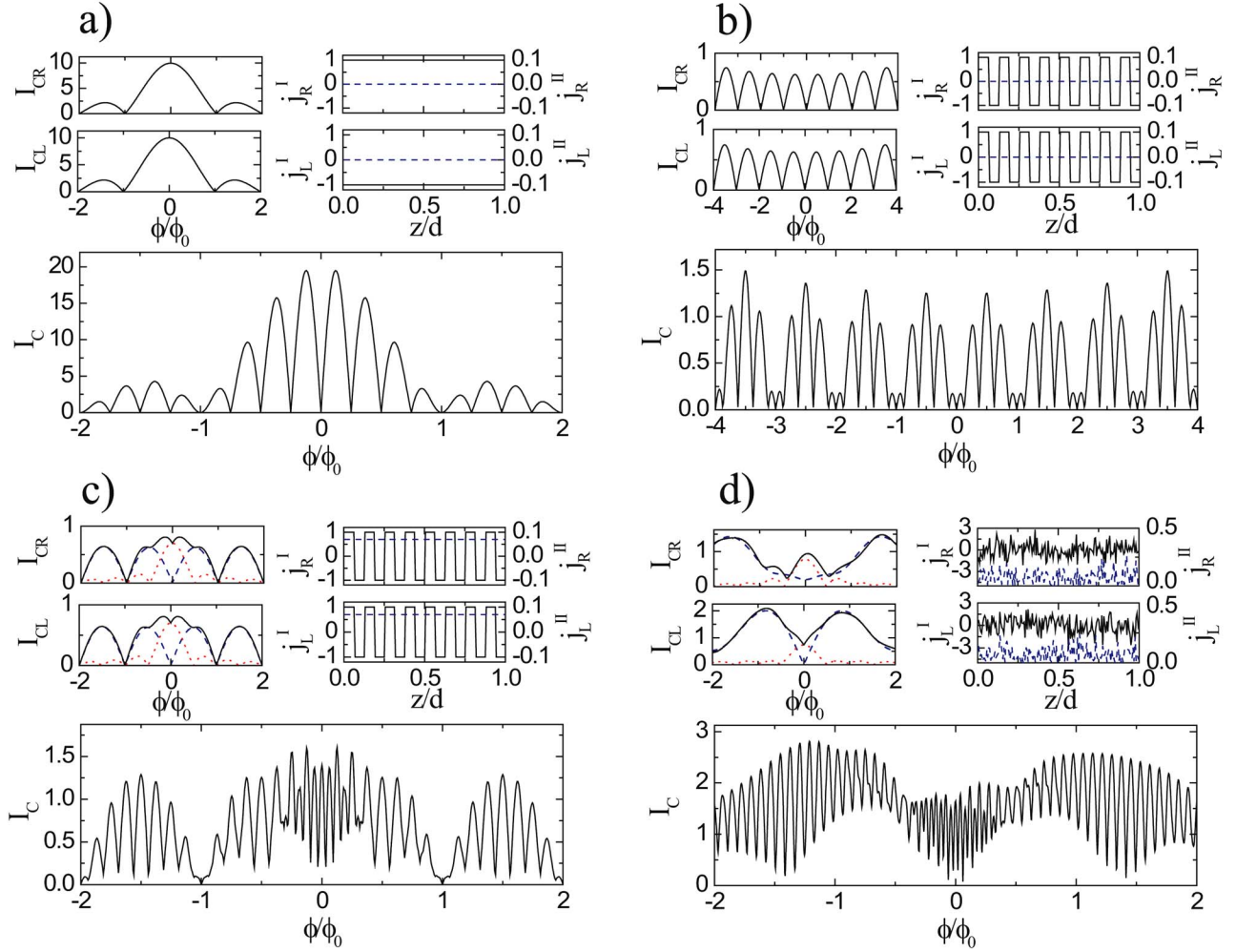


FIG. 4. (Color online) Examples of simulated I_c vs ϕ patterns showing the effects of π -facets and the addition of a second-harmonic current component to the CPR. To each I_c vs ϕ pattern four insets are attached. The left insets present the corresponding I_c vs ϕ pattern for the SQUIDs/junctions and the ones to the right the current distributions $J_c(z)$ for the first- (full lines) and second- (dashed lines) harmonic current components of each junction, respectively. J_{c0}^I was set to 1 kA/cm² in all four cases except for (d) where the average of J_{c0}^I equals 1 kA/cm². In (c) and (d) J_{c0}^I and the average J_{c0}^{II} are set to 80 A/cm². In (a) a π -SQUID is modeled. In the right inset one can see that the sign of J_c for the two junctions differs. The I_c vs ϕ pattern has a minima at zero field but the envelope of the SQUID and its junctions has a conventional shape. (b) The I_c vs ϕ pattern for a so-called zig-zag junction. The GB is modeled by letting every second facet be a π -facet, which causes the resulting current distribution to alternate between $+J_{c0}$ and $-J_{c0}$. In (c) a second-harmonic current component is added to the zig-zag model described above. The current distribution for the second harmonic is constant and the I_c vs ϕ pattern for the SQUID show π -periodic features. In (d) the results for a SQUID with stochastic current distribution are shown. The meandering of the GB causes J_c^I and J_c^{II} to fluctuate. The pattern is highly asymmetric and in qualitative agreement with experimental data. We are able to see how the first harmonic and second harmonic via Eq. (1) add up to an envelope. This methodology can be transferred to the more complex I_c vs ϕ pattern of the SQUID. The effects of the second harmonic are most visible at zero magnetic field where it has its global maxima, but are manifested at higher fields as well.

a so-called π -SQUID,²⁹ i.e., a dc-SQUID with a conventional CPR and one conventional (“0”) junction and one π -junction. The resulting pattern shown in Fig. 4(a) has a minimum at zero field but a junction envelope with a conventional shape.

c. $J_{k=L,R}^I(z) = J_{c0}^I [\sum_{m=0}^N 2(-1)^m \Theta(z - a \cdot m) - 1]$, $J_{k=L,R}^{II}(z) = 0$, where $\Theta(z)$ is the Heaviside step function, $N_{k=L,R}$ denotes the number of facets, and a the typical length of each facet so that $d = a \cdot N$. This is the so-called zig-zag model of a GB discussed by Smilde *et al.*³⁰

The net effect of the faceting is modeled by incorporating a phase shift of π for every second facet, i.e., $J_c > 0$ for the

0-facets and $J_c < 0$ for the π -facets. For a SQUID possessing identical junctions with even number of facets I_s is given by

$$I_s(\Phi) = \max_{-\pi < \phi_0 < \pi} \frac{J_{c0}^I wd}{\frac{\pi \Phi}{\Phi_0}} \left\{ 2 \sum_{m=0}^{N/2} \left[(-1)^m \cos\left(\frac{2\pi \Phi m}{\Phi_0 N}\right) \right] - 1 - \cos\left(\frac{\pi \Phi}{\Phi_0}\right) \right\} (\cos(\phi_0) + \cos(\phi_0 + \phi_x)). \quad (6)$$

TABLE I. The parameters for the dc-SQUIDs used in this work. All parameters are at 4.2 K and zero magnetic field.

Sample	Junction width (μm)	I_c μA	Area μm^2	L pH	β_L	Type
SQ1	2	4.7	15×15	41	0.19	$0^\circ\text{--}45^\circ$
SQ2	4	18	5×5	11	0.20	$0^\circ\text{--}45^\circ \pm 10^\circ$
SQ3	1	1.5	7×7	19	0.03	$0^\circ\text{--}45^\circ + 45^\circ$
SQ4	4	29	10×10	24	0.70	$0^\circ\text{--}45^\circ + 45^\circ$
SQ5	2	10	10×10	26	0.26	$0^\circ\text{--}45^\circ + 45^\circ$
SQ6	2	1.5	5×5	12	0.02	$0^\circ\text{--}45^\circ \pm 10^\circ$

Note that I_s vanishes at zero field (since the $N/2+1$ elements in the sum equals $+2$ at zero field and the remaining two terms equal -2), and that its maximum occurs at nonzero field. One should also note that the magnetic diffraction pattern is a superposition of cosine terms with frequencies $(2\pi\Phi/\Phi_0)n/N$, $n=0,1,\dots,N/2$. Thus the behavior in a magnetic field acts at many different length scales simultaneously. When incorporated in a SQUID, the result is as shown in Fig. 4(b). Note that this special case can only be realized using hybrid sd junctions (in the work by Smilde *et al.* a Nb-YBCO junction was used). There is no second-harmonic current component since it is assumed that only lobe-to-lobe tunneling is involved.

d. $J_{k=L,R}^I(z) = J_{c0}^I [\sum_{m=0}^N 2(-1)^m \Theta(z - a \cdot m) - 1]$, $J_{k=L,R}^{II}(z) = J_{c0}^{II}$. This is the simplest model for the behavior of asymmetric high-angle GB junctions with faceting and a second-harmonic component in the CPR. An illustration of the geometry and corresponding current distribution can be seen in Fig. 3(a). In the example shown in Fig. 4(c) calculated for a symmetric SQUID the faceting causes the first harmonic to alternate sign and behave as in the previous example, the difference being that we now assume that the angle of the facets deviates slightly from 45° leaving a nonzero first-harmonic component. Since the second harmonic is π -periodic $J_{k=L,R}^{II}(z) = \text{constant}$, the second harmonic will form a Fraunhofer pattern with periodicity $2\pi\Phi/\Phi_0$. Thus, the effect on the SQUID pattern will be evident at low field but also at higher field where I^I/I^II is sufficiently large.

e. $J_{k=L,R}^I(z) = J_{c0,k=L,R}^I \chi(z)_{k=L,R}$, $J_{k=L,R}^{II}(z) = J_{c0,k=L,R}^{II} \vartheta(z)_{k=L,R}$. This is the most realistic model of a real GB. The interface structure is depicted in Fig. 3(b). The meandering of the GB

causes J_c to fluctuate and so does the relative magnitudes of the harmonics. $-1 < \chi_{k=L,R} < 1$ and $0 < \vartheta_{k=L,R} < 1$ are stochastic variables. Assuming that the properties change appreciably on a scale set by the length of a facet ~ 100 nm, this would mean that the dynamics of a SQUID with $4 \mu\text{m}$ junctions is described by 80 independent variables. In general, these SQUIDs are asymmetric also with respect to the average $\langle J_c \rangle$ and the effective value of α in each junction. In the example shown in Fig. 4(d) the influence of the second harmonic is manifested at low field and the π -faceting causes the maximum I_c to be shifted to nonzero fields. This example also demonstrates that the effects of the second harmonic are only visible through the lack of B symmetry and through small modulations at certain fields that sometimes disappear altogether when the field strength is increased.

Due to the complex nature of the GB, it is difficult to extract reliable values for each current component from experimental I_c vs ϕ patterns. We have previously shown that it is indeed possible to mimic the behavior numerically by using a curve fitting procedure with good result.¹¹ One should be aware, though, that since there are many free parameters it is possible to obtain a solution which is not necessarily the true one. Another tempting method would be to use a Fourier transform. However, the nature of the Fourier transform requires a SQUID with identical junctions in order to extract the current components accurately. Furthermore, since the current is proportional to the maximum of the CPR the spectrum is very complex. Even in the case of a SQUID with a conventional CPR we have $I \propto |\sin(\Omega t)|$ resulting in a spectrum which consists of a set of frequency peaks. Thus, in general it is not possible to extract anything more than qualitative information about the presence of a second harmonic from the spectrum without the use of special phase retrieval algorithms.^{31,32}

Note also that the model outlined here does not include the effects of thermal noise. Since $0^\circ\text{--}45^\circ$ junctions always have relatively low critical currents (of the order of a few μA) thermal smearing of the I - V characteristics is an issue even at 4.2 K. Hence, this effect needs to be taken into account when interpreting temperature-dependent data.

III. SAMPLE FABRICATION AND MEASUREMENT TECHNIQUES

All samples used in this work were fabricated on SrTiO₃ bicrystals using our standard amorphous carbon process.^{33,34}

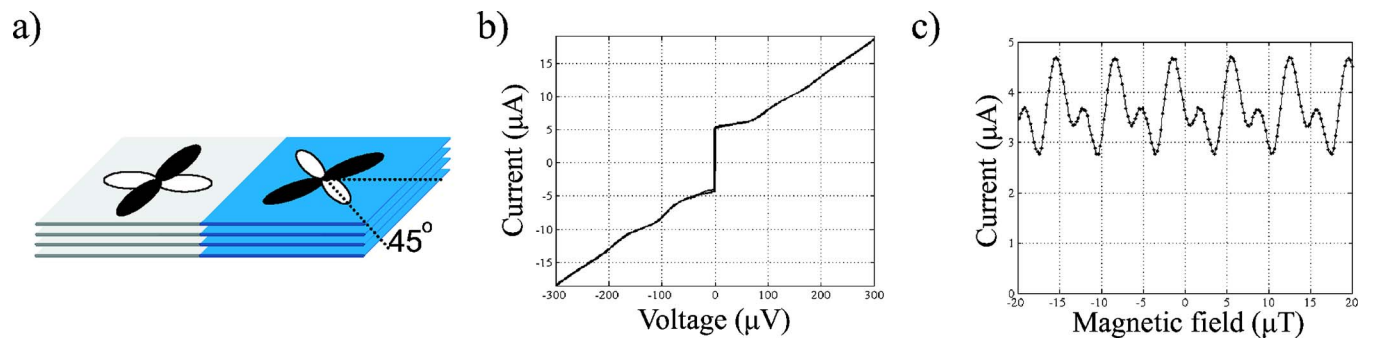


FIG. 5. (Color online) Geometry, I - V curve, and modulation of SQ1 which is a dc-SQUID fabricated on an ordinary $0^\circ\text{--}45^\circ$ [001]-bicrystal and measured at 4.2 K.

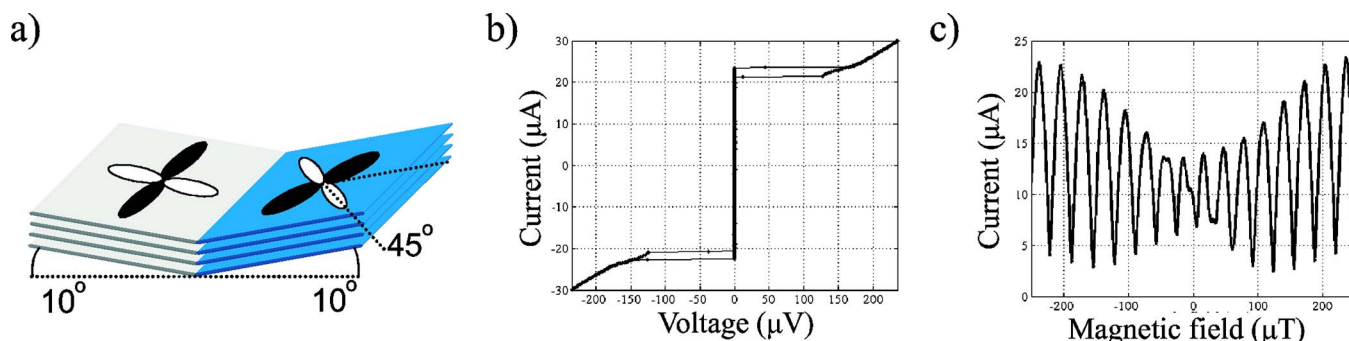


FIG. 6. (Color online) Geometry, I - V curve, and modulation of the device denoted SQ2, a 0° - $45^\circ \pm 10^\circ$ SQUID, measured at 50 mK. This device was made with $4\text{-}\mu\text{m}$ -wide junctions resulting in the junction modulation being visible on the same field scale as the SQUID modulation.

Three different types of bicrystals were used: 45° [001] tilt and 45° [001] tilt with an additional 45° or 10° [100] tilt. The latter will be referred to as tilt-tilt. In Table I we use the notation α - β + γ for a bicrystal formed by an α - β misorientation angle with respect to the [001] axis and an additional tilt γ with respect to the [100] axis.

The main idea behind fabricating such new bicrystal substrates is that in a tilt-tilt GB the direction of current flow is potentially in the c -axis direction, this has been shown to lead to highly hysteretic junctions.¹⁹ The geometry of the samples used in this work can be seen in Figs. 5(a), 6(a), and 7(a).

The fabrication starts by the deposition of a 250 nm YBCO film using pulsed laser deposition. The film is capped *in situ* with a 20 nm layer of gold. Another layer of 30 nm of gold is then deposited *ex situ*.

Contact pads and alignment marks are first patterned in a 200 nm Au film using an e-beam lithography lift-off process. Fine rulers ($0.5\ \mu\text{m}$ pitch) are also defined in the same step to enable the optical localization of the GB. The design of the chip is adjusted according to the actual GB position on the chip thus allowing a $0.2\ \mu\text{m}$ positioning accuracy of the pattern with respect to the GB. We then deposit an amorphous carbon layer (120 nm) by e-beam evaporation. The chip design is patterned onto a Cr mask by lift-off. The pattern is then transferred to the a -C mask by oxygen plasma etching through the Cr mask. The YBCO film is then ready to be etched by Ar ion milling through the positive a -C mask. The final stage involves stripping the residual a -C

mask and Au layer covering the YBCO, rendering devices ready for measurement.

The loop sizes and junction widths were effectively determined by the requirement that the junctions should not modulate appreciably in the same field range as the SQUID response. Moreover, all devices were designed to have a junction width $d \ll \lambda_J$ in order to avoid complications due to self-generated flux,³⁵ which is known to affect the dynamics of long junctions.³⁶

The samples were measured using two different measurement setups. Both systems are magnetically shielded and located in EMI-shielded rooms. For measurements in the temperature range 0.3–30 K we used an Oxford Instruments Heliox VL ^3He system. An Oxford Model 200 dilution refrigerator was used for measurements down to 15 mK. The critical current was measured by ramping the current and detecting when the voltage exceeded a voltage criterium, the latter being determined by the noise level and the shape of the I - V curve; usually a value of 5–15 μV was used.

One complication in designing and characterizing these devices is that in order to unambiguously say that the dynamics is affected by a second-harmonic current component, the SQUID should be asymmetric both with respect to $I_{cR,cL}$ and $\alpha_{L,R}$. Due to the meandering of the GB, there is usually a relatively large spread in critical current between junctions fabricated on 0° - 45° bicrystal substrates; the total critical current can vary by as much as a factor of 2–3 even between two nominally identical junctions. Therefore, even though the samples are symmetric by design, there is usually enough

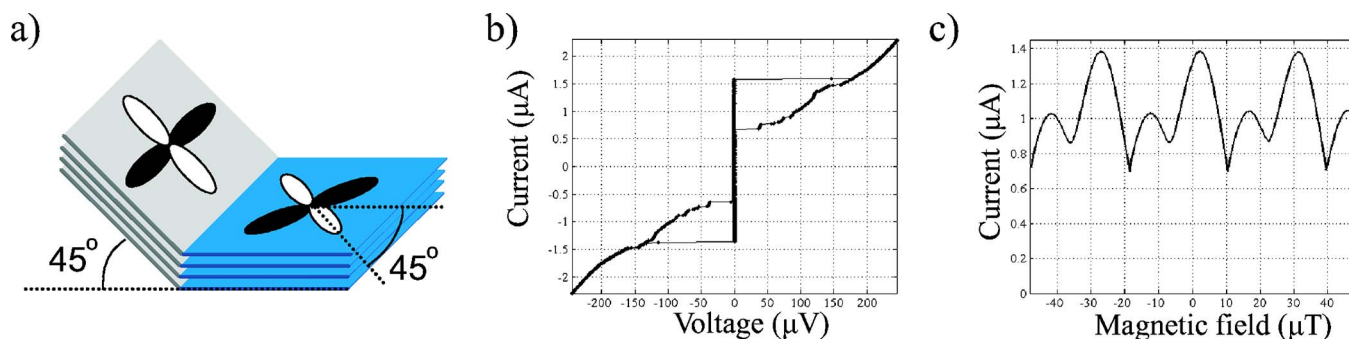


FIG. 7. (Color online) Geometry, I - V curve, and modulation of SQ3 at 50 mK. Due to the 45° [100] tilt the SQUID is underdamped. The shape of the SQUID modulation indicates the presence of a strong second-harmonic component in the CPR of the junctions.

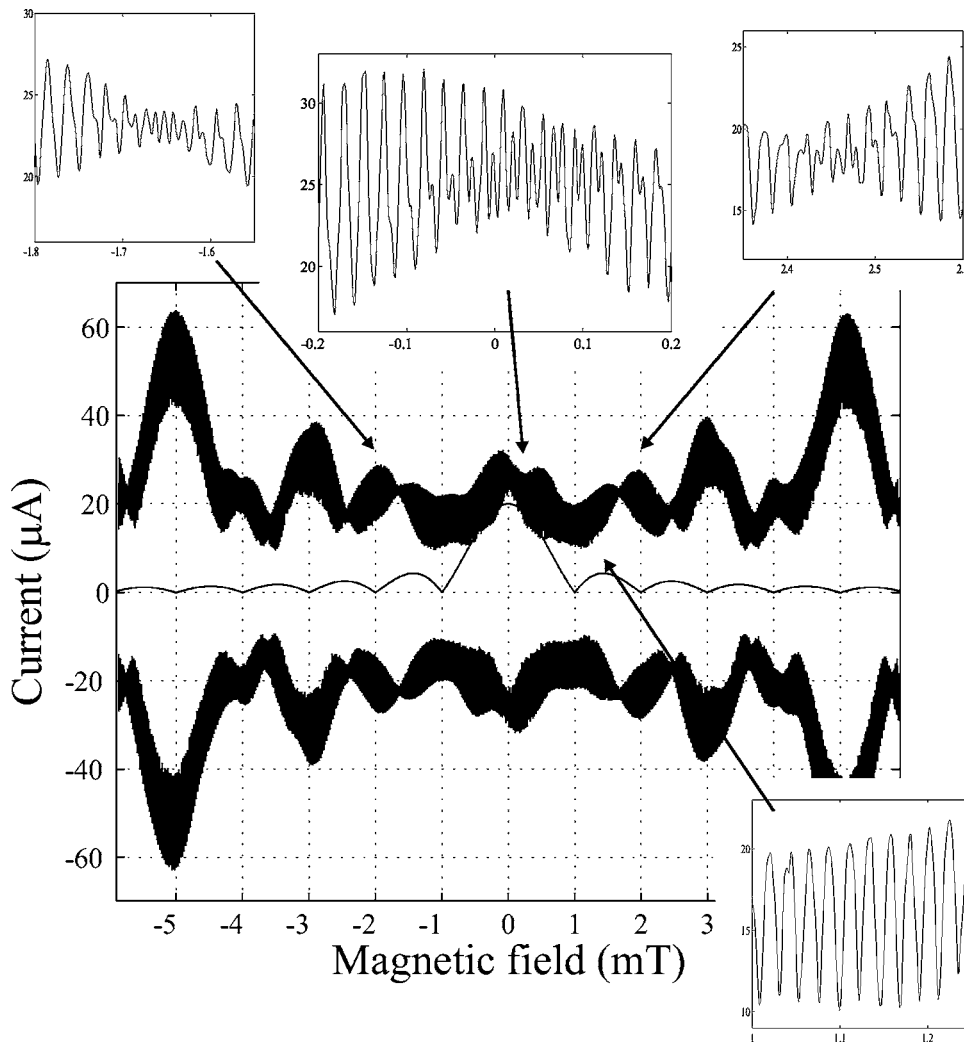


FIG. 8. Measurements at large field of sample SQ4 at 4.2 K. The insets show the behavior around zero field as well as at elevated fields. At around 1.1 mT the π -periodic feature is no longer visible but it reappears again at 1.7 and 2.5 mT, these values correspond to maxima of the second harmonic. Shown for comparison is also the pattern one would expect from a SQUID with uniform junctions and a CPR with no first-harmonic component, $I = I^{\text{II}} \sin 2\phi$.

parameter spread to clearly show the effects we are interested in.

IV. MEASUREMENTS

We have performed measurement on a wide variety of samples. Here we will present data from six SQUIDs with different geometries fabricated on three different bicrystals. The samples are denoted SQ1–SQ6 and the parameters can be found in Table I.

The properties of SQUIDs fabricated on ordinary [001]-tilt bicrystals were discussed in our previous work¹¹ and the results shown in Fig. 5 are very similar to those already presented there. The current-voltage (I - V) characteristics and the modulation shows that the SQUID is overdamped and exhibits an anomalous current modulation with a clear second-harmonic component. The shape of the modulation, similar to the numeric result shown in Fig. 2, also shows that the SQUID is asymmetric with respect to the properties of the junctions despite having a geometry where the junctions are nominally identical.

The main difference between the samples fabricated on ordinary bicrystals and the novel tilt-tilt type is that the latter exhibits hysteretic current-voltage characteristics. This can

be seen in Fig. 6, which shows a measurement of a SQUID fabricated on a bicrystal with a ± 10 [100] tilt added in addition to the 45° [001] tilt. The change in current voltage characteristics is presumably due to the c -axis transport. A small amount of doubling is present in the field modulation.

When the [100] tilt is increased even further to 45° as in Fig. 7 the SQUIDs generally become highly hysteretic and have a relatively large Q value.³⁷ Using the Zappe approximation for the Stuart-MacCumber parameter³⁸ we get

$$\beta_c \approx \frac{2 - (\pi - 2)(I_r/I_c)}{(I_r/I_c)^2} \approx 7.4.$$

Whereas hysteretic SQUIDs fabricated on conventional [001] bicrystals exhibit ordinary modulation¹⁵ we now retain the same type of analogous modulation as in Fig. 5. This demonstrates that the presence of a strong second-harmonic component does not preclude devices with high Q values.

By applying higher fields it is possible to examine the field dependence of the junctions. Figure 8 shows a measurement of the SQUID denoted SQ4 at large fields where the modulation due to the junctions is visible. The fact that we only have a local minimum (as opposed to a global maximum) in the center implies that π -facets are indeed present

in the GB. Without the contribution of negative currents, there is always a global maximum at zero field. π -periodic features are only visible at certain values of the applied field where the I^{II}/I^I ratio is large enough. As pointed out in Sec. II this is most likely to happen when the second harmonic has a maximum.

The insets of Fig. 8 show the SQUID modulation in different field ranges. A π -periodic feature is visible near zero field, but the SQUID modulation has a conventional shape at slightly higher fields. This behavior is similar to the numerical result shown in Fig. 4(d). When the field strength is increased to 1.5 mT π -periodic features are again visible since the second maximum of the second-harmonic current component is reached.

V. COMPARISON BETWEEN SQUID AND INDIVIDUAL JUNCTION DATA

As has already been pointed out it is very difficult to extract any quantitative information about the properties of the junctions from studying the SQUID response. This is due to the large number of free variables involved which means that there are several sets of parameters that fit the data equally well. In order to verify that the anomalous modulation we see in our experiments can indeed be attributed to properties of the junctions themselves, we fabricated SQUIDS where one electrode was split into two branches. This made it possible to first characterize the SQUID and then separate the junctions by cutting the loop into two using a focused ion beam (FIB), so that both junctions could be measured independently. This drastically reduces the number of free variables and we are left to determine α_L and α_R by fitting the data to Eq. (2).

We present data from the device denoted SQ1 in Fig. 9. The SQUID had a maximum critical current of $4.6 \mu\text{A}$ and a normal resistance 17Ω at 4.2 K. The measured periodicity of the SQUID deviates 37% from what one would expect from the hole area, we attribute this to a flux-focusing effect (the effective area of the SQUID corresponds to $16.8 \times 16.8 \mu\text{m}^2$, which is in good agreement with numerical simulations³⁹).

To avoid gallium poisoning of the GB during the etching, a dual-beam FIB was used to cut the loop. All imaging was then done using the integrated scanning electron microscope and the total dose to the GB was minimal. The junctions were located approximately $10 \mu\text{m}$ from the point where the cut was made. The junctions were characterized at 4.2 K and were found to have critical currents of 3.1 and $1.1 \mu\text{A}$, respectively. These values did not change appreciably in the magnetic field range used here. The normal resistances were about 40 and 37Ω , consistent with the resistance of the SQUID.

In order to fit the data we assume that the SQUID has a field-dependent CPR of the form given by Eq. (2) and that the critical current of each junction is given by $\max_{\phi}\{I^I \sin \phi - I^{II} \sin 2\phi\}$.

The solid lines in Fig. 9 show the result of a fit to Eq. (2). In order to fit the data we have used $I_{cL}=3.5 \mu\text{A}$, $I_{cR}=1.1 \mu\text{A}$, $\alpha_L=4.2$, and $\alpha_R=0.72$. Using these parameters fit

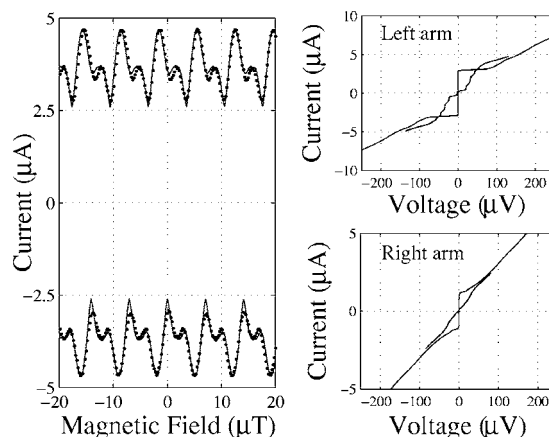


FIG. 9. Measurements of a three-electrode device before and after the loop was cut using a FIB at 4.2 K. The SQUID modulation as well as the I - V curves of the junctions of the left and right arms are shown. The full lines in the left figure are fitted using $\alpha_R=0.72$ and $\alpha_L=4.2$, respectively. A background field of approximately $2.2 \mu\text{T}$ is assumed in order to fit the data. The I - V characteristics of the junctions under 5 GHz microwave irradiation are also shown. Shapiro steps are easily distinguished.

to calculate the critical currents of the junctions we get values of the critical currents that are about 10% higher than those actually measured. Note that the *maximum* current of the modulation is given by the usual expression $I_{\max}=I_{cL}+I_{cR}$ and is not related to the values of $\alpha_{L,R}$. No excess current was used to fit the data. This is consistent with the fact that the supercurrent in both junctions could be almost completely suppressed using microwave irradiation. Several Shapiro steps were seen in the I - V characteristics of both junctions.

VI. TEMPERATURE DEPENDENCE OF THE CURRENT MODULATION

Since the first and second harmonics in Eq. (1) are carried via different transport mechanisms, they have different temperature dependencies.^{40,6} The channels that carry the $\sin 2\phi$ component will have a negligible J_c at temperatures $k_B T > D|\Delta|$, Δ being the superconducting gap and D the transparency of the junction, but can dominate the transport through the junction at low temperatures. This results in a strong temperature dependence of the effective CPR (see, e.g., Refs. 41 and 1). The exact behavior is difficult to predict since it depends on the local properties of the GB and these are not directly accessible in experiments. The distribution of misorientation angles and local transparency, the presence of impurities/vacancies in the GB, the shape of the tunneling cone, vary over the length of the junction. Thus, the exact temperature dependence will be sample dependent.

In Fig. 10 we show data from the SQUID denoted SQ5. As expected the SQUID has a conventional modulation at high temperatures but as the temperature is lowered below 15 K the π -periodic feature starts to be clearly visible. As the temperature is decreased even further this feature grows until a well developed “hump” becomes visible. As was noted

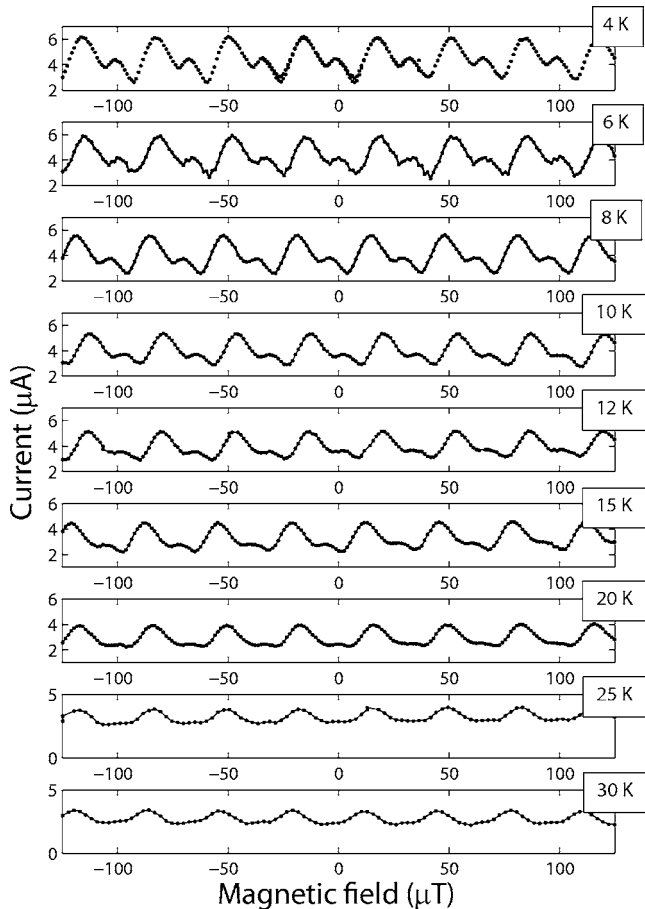


FIG. 10. Temperature dependence of the I_c - B pattern for sample SQ5. At 30 K the modulation is close to a conventional shape, but as the temperature is lowered a π -periodic component becomes visible and is clearly seen at temperature below 15 K.

above it is hard to extract the current components from the modulation meaning it is difficult to quantify the temperature dependence. However, the temperature range where the feature becomes significant, 15–20 K, is consistent with previous results by Il'ichev *et al.*⁶

When both junctions and the SQUID modulate in the same magnetic field range, the temperature-dependent data will look like in Fig. 11. It shows critical current measurements on the SQUID denoted SQ6 between 50 mK and 11.5 K. When the temperature is decreased, new features appear at fields corresponding to twice the usual frequency. The pattern becomes highly irregular since the dynamics of both the junctions and the SQUID are affected by the second harmonic.

In this sample the effects of the second harmonic were only visible at very low temperatures. This is consistent with the low critical current value since this implies a low transparency interface. It is also in agreement with the results presented in Ref. 10 where the onset temperature was reported to be below 1 K for a junction with an average junction transparency 10^{-4} .

VII. SUMMARY AND CONCLUSION

0° – 45° GB dc-SQUIDs are very complex devices. The critical current of nominally identical junctions can vary by a

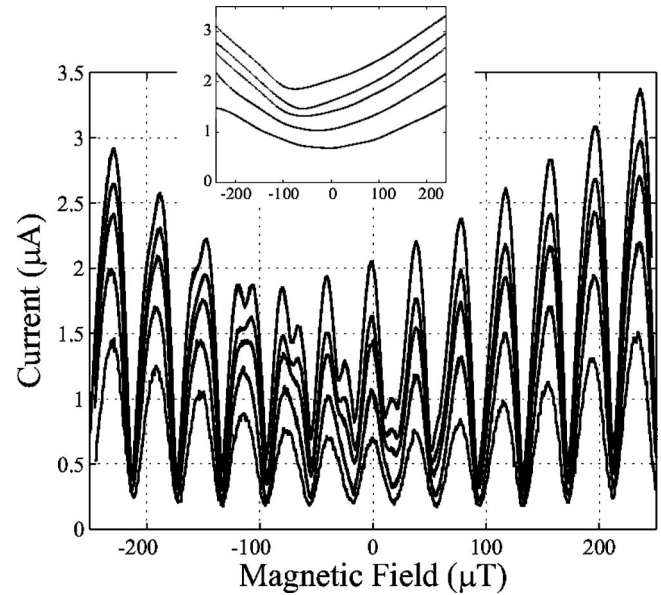


FIG. 11. Critical current modulation of SQUID SQ6 at four different temperatures. *From top to bottom*: 50 mK, 4.2, 7.2, 9.1, and 11.5 K. Note how the envelope in the inset changes as the temperature decreases. This change shows that the second harmonic in the CPR not only affects the SQUID modulation but also the magnetic diffraction patterns of the junctions.

factor of 2–3 and the amplitude of the second-harmonic Josephson current component varies by a factor of 4 in our experiments. This implies different local structures of the GB which are reflected both in the number of π -facets and the relative magnitude of the harmonics of the effective CPR of each junction. Furthermore, low-angle facets can completely dominate the current transport since the local critical current density is angle-dependent due to the d -wave symmetry. A large value of α is only possible where these facets are absent *or* the effective magnitude of the conventional Josephson current is reduced due to π -facets. It is therefore not surprising that the junctions of SQUIDs that show a strong effect of the second-harmonic Josephson current often have I_c vs ϕ patterns which are asymmetric with respect to zero field and have a minimum in the center (the pattern is, however, always point symmetric). The minima can be attributed to the presence of π -facets and the asymmetry to the second-harmonic term (assuming flux trapping can be ruled out in the experiment). It is often the case in both experiments and simulations that any visible π -periodic features of the SQUID modulation disappears when the strength of the applied field is increased. This is due to the two current components in the junctions having different field dependencies, essentially the magnetic diffraction patterns of the first- and second-harmonic currents are different, which is reflected in the resulting total interference pattern of the SQUID. This is consistent with the reasoning above and the fact that the features often reappear as the strength of the field is increased even further. Hence, the stochastic nature of a real GB means that a high-angle HTS junction incorporates many different effects; all of which can be attributed to the d -wave symmetry of the pairing wave function.

The temperature dependence of the modulation is consistent with the first- and second-harmonics of the CPR having

different temperature dependencies.⁴² That we see a strong effect of the second harmonic up to temperatures of 15 K implies a relatively large transparency D of the junctions despite the low critical current. However, there is a large discrepancy between indirect measurements of the effective D of the junction via the normal resistance and what can be inferred from the relative magnitude of the harmonics using microscopic theory. Again, this is probably due to the fact that most theories do not take the complicated nature of the GB into account.

In order to utilize the effects of the unconventional CPR in the quantum regime we need underdamped junctions. However, in our previous experiments with conventional [001]-tilt bicrystals, all structures that exhibited strong second-harmonic behavior were overdamped. On the other hand, bicrystals with both [001] and [100] tilt seem to be almost ideal for this type of experiment as has been shown here. We can only speculate about the reason for the difference in behavior at this point. Theoretically, a strong second-harmonic contribution implies junctions with high transparency, which is at odds with a tunnel-like behavior. It is not clear how the transport is changed by the additional [100] tilt, if it simply changes the properties of the interface or if the effect is related to more fundamental properties such as the orientation of the tunneling cone with respect to the pairing wave function.

The intrinsic dissipation in this type of junction might not spell doom for a d -wave qubit. However, it is important to remember that there are many other sources of dissipation in a Josephson junction and many of these—such as the presence of two-level fluctuators in the barrier—are difficult to

control even when using junctions fabricated from conventional superconductors, despite using well-established fabrication processes. Hence, it is therefore possible that such effects will also be what ultimately limits the performance of any real implementation of a HTS qubit. At the time of this writing we can only conclude that more research is needed before we can answer these questions.

Although there are still some unanswered questions which warrant further investigation we now believe we have a good understanding of the dynamics of 0° – 45° GB dc-SQUIDS. As long as all the relevant effects are properly taken into account theory is in qualitative agreement with experiment. Our experimental results are encouraging and indicate that the tilt-tilt bicrystal is a promising candidate for experiments with HTS structures in the quantum regime. By increasing the [100] tilt of the bicrystals we increase the hysteresis of SQUIDS and we attribute the relatively high Q value to the c -axis transport. The unconventional CPR can give rise to a doubly degenerate ground state. These devices are potentially very interesting for qubit applications.

ACKNOWLEDGMENTS

We would like to thank Mattias Torstensson for his help with the FIB. We would also like to thank Tord Claeson, Carol Webster, and Alexander Ya. Tzalenchuk for valuable discussions and comments. Support was given by the Swedish Research Council (VR), International Science and Technology Center (ISTC), and the Swedish Foundation for Strategic Research (SSF).

*Current address: National Physical Laboratory, Queens Road, Teddington, Middlesex TW11 0LW, UK. Electronic address: tobias.lindstrom@npl.co.uk

¹T. Löfwander, V. Shumeiko, and G. Wendin, *Supercond. Sci. Technol.* **14**, R53 (2001).

²C.-R. Hu, *Phys. Rev. Lett.* **72**, 1526 (1994).

³S. K. Yip, O. F. deAlcantaraBonfim, and P. Kumar, *Phys. Rev. B* **41**, 11214 (1990).

⁴A. Zagoskin, *J. Phys.: Condens. Matter* **9**, 419 (1997).

⁵H. Hilgenkamp and J. Mannhart, *Rev. Mod. Phys.* **74**, 297 (2002).

⁶E. Il'ichev, V. Zakosarenko, R. P. J. Ijsselsteijn, H. E. Hoenig, V. Schultze, H.-G. Meyer, M. Grajcar, and R. Hlubina, *Phys. Rev. B* **60**, 3096 (1999).

⁷E. Il'ichev, V. Zakosarenko, V. Schultze, H.-G. Meyer, H. Hoenig, V. Glyantsev, and A. Golubov, *Appl. Phys. Lett.* **72**, 731 (1998).

⁸A. Golubov, M. Kupriyanov, and E. Il'ichev, *Rev. Mod. Phys.* **76**, 411 (2004).

⁹J. Komiya, H. D. Chen, C. Zhang, and Y. Ando, *Phys. Rev. Lett.* **94**, 207004 (2005).

¹⁰T. Bauch, F. Lombardi, F. Tafuri, A. Barone, G. Rotoli, P. Delsing, and T. Claeson, *Phys. Rev. Lett.* **94**, 087003 (2005).

¹¹T. Lindström, S. A. Charlebois, A. Y. Tzalenchuk, Z. Ivanov, M.

H. S. Amin, and A. M. Zagoskin, *Phys. Rev. Lett.* **90**, 117002 (2003).

¹²C. Schneider, G. Hammerl, G. Logvenov, T. Kopp, J. Kirtley, P. J. Hirschfeld, and J. Mannhart, *Europhys. Lett.* **68**, 88 (2004).

¹³C. Gardiner, R. Lee, J. Gallop, A. Tzalenchuk, J. Macfarlane, and L. Hao, *Supercond. Sci. Technol.* **17**, 234 (2004).

¹⁴M. H. S. Amin, A. Y. Smirnov, A. M. Zagoskin, T. Lindström, S. A. Charlebois, T. Claeson, and A. Y. Tzalenchuk, *Phys. Rev. B* **71**, 064516 (2005).

¹⁵S. Charlebois, T. Lindström, A. Tzalenchuk, Z. Ivanov, and A. Zagoskin, *Physica C* **408-410**, 926 (2004).

¹⁶S. Kawabata, S. Kashiwaya, Y. Asano, and Y. Tanaka, *Phys. Rev. B* **72**, 052506 (2005).

¹⁷M. H. S. Amin and A. Y. Smirnov, *Phys. Rev. Lett.* **92**, 017001 (2004).

¹⁸T. Bauch, T. Lindström, F. Tafuri, G. Rotoli, P. Delsing, T. Claeson, and F. Lombardi, *Science* **311**, 57 (2006).

¹⁹F. Lombardi, F. Tafuri, F. Ricci, F. Miletto Granozio, A. Barone, G. Testa, E. Sarnelli, J. R. Kirtley, and C. C. Tsuei, *Phys. Rev. Lett.* **89**, 207001 (2002).

²⁰Y. Divin, U. Poppe, C. Jia, P. Shadrin, and K. Urban, *Physica C Fifth European Conference on Applied Superconductivity, EUCAS 2001*, 26–30 Aug. 2001, Vol. 372-376, p. 115.

²¹E. Sarnelli, G. Testa, D. Crimaldi, M. A. M. Adamo, and N. M.

- A., IEEE Trans. Appl. Supercond. **15**, 245 (2005).
- ²²S.-W. Chan, Q. Jin, J. Tsai, S. Tidrow, and Q. Jiang, IEEE Trans. Appl. Supercond. **13**, 2829 (2003).
- ²³J. Mannhart and P. Chaudhari, Phys. Today **54**, 48 (2001).
- ²⁴In a microscopic theory the length scale would be set by ξ_0 , the superconducting coherence length which is 1.5 nm in YBCO, much smaller than the length of the facets ~ 100 nm. Hence, the properties of each channel in our model are really the average taken over many (microscopic) channels meaning we assume that the properties only change appreciably on a length scale set by the facet length.
- ²⁵V. Kornev, I. Soloviev, N. Klenov, N. Pedersen, I. Borisenko, P. Mozhaev, and G. Ovsyannikov, IEEE Trans. Appl. Supercond. **13**, 825 (2003).
- ²⁶W. Neils and D. van Harlingen, Physica B **284-288**, 587 (2000).
- ²⁷N. Lazarides, Supercond. Sci. Technol. **17**, 585 (2004).
- ²⁸See, e.g., A. M. Kadin, *Introduction to Superconducting Circuits* (Wiley, New York, 1999).
- ²⁹D. A. Wollman, D. J. VanHarlingen, W. C. Lee, D. M. Ginsberg, and A. J. Leggett, Phys. Rev. Lett. **71**, 2134 (1993).
- ³⁰H. J. H. Smilde, D. H. A. Arlando Blank, G. J. Gerritsma, H. Hilgenkamp, and H. Rogalla, Phys. Rev. Lett. **88**, 057004 (2002).
- ³¹M. Carmody, L. Marks, and K. Merkle, Physica C **315**, 145 (1999).
- ³²M. Carmody, B. Moeckly, K. Merkle, and L. Marks, J. Appl. Phys. **87**, 2454 (2000).
- ³³A. Tzalenchuk, T. Lindström, S. Charlebois, E. Stepantsov, A. Zagoskin, Z. Ivanov, and T. Claeson, IEEE Trans. Appl. Supercond. **13**, 948 (2003).
- ³⁴A. Tzalenchuk, T. Lindström, S. Charlebois, E. Stepantsov, Z. Ivanov, and A. Zagoskin, Phys. Rev. B **68**, 100501 (2003).
- ³⁵J. Mannhart, H. Hilgenkamp, B. Mayer, C. Gerber, J. R. Kirtley, K. A. Moler, and M. Sgrist, Phys. Rev. Lett. **77**, 2782 (1996).
- ³⁶R. G. Mints, Phys. Rev. B **57**, R3221 (1998).
- ³⁷Note that the Q value determined from the dc characteristics of a device can differ significantly from the spectroscopic Q value in the quantum regime, the latter must be determined using spectroscopy.
- ³⁸H. Zappe, J. Appl. Phys. **44**, 1371 (1973).
- ³⁹M. Khapaev, A. Kidiyarova-Shevchenko, P. Magnelind, and M. Kupriyanov, IEEE Trans. Appl. Supercond. **11**, 1090 (2001).
- ⁴⁰Y. S. Barash, H. Burkhardt, and D. Rainer, Phys. Rev. Lett. **77**, 4070 (1996).
- ⁴¹S. Kashiwaya and Y. Tanaka, Rep. Prog. Phys. **63**, 1641 (2000).
- ⁴²Y. S. Barash, Phys. Rev. B **61**, 678 (2000).